10-21-2018

Magnetic and Electrocatalytic Properties of Transition Metal Doped MoS_2 Nanocrystals

Karthik Chinnathambi
Boise State University

Magnetic and electrocatalytic properties of transition metal doped MoS_2 nanocrystals

L. M. Martinez,[1,a)] J. A. Delgado,[1,a)] C. L. Saiz,[1] A. Cosio,[1] Y. Wu,[2] D. Villagrán,[2] K. Gandha,[3] C. Karthik,[4] I. C. Nlebedim,[3] and S. R. Singamaneni[1,b)]
[1]*Department of Physics, The University of Texas at El Paso, El Paso, Texas 79968, USA*
[2]*Department of Chemistry and Biochemistry, The University of Texas at El Paso, El Paso, Texas 79968, USA*
[3]*Critical Materials Institute, Ames Laboratory, Ames, Iowa 50011, USA*
[4]*Micron School of Materials Science and Engineering, Boise State University, 1910 University Drive, Boise, Idaho 83725, USA*

(Received 6 June 2018; accepted 18 September 2018; published online 17 October 2018)

In this paper, the magnetic and electrocatalytic properties of hydrothermally grown transition metal doped (10% of Co, Ni, Fe, and Mn) 2H-MoS_2 nanocrystals (NCs) with a particle size 25–30 nm are reported. The pristine 2H-MoS_2 NCs showed a mixture of canted anti-ferromagnetic and ferromagnetic behavior. While Co, Ni, and Fe doped MoS_2 NCs revealed room temperature ferromagnetism, Mn doped MoS_2 NCs showed room temperature paramagnetism, predominantly. The ground state of all the materials is found to be canted-antiferromagnetic phase. To study electrocatalytic performance for hydrogen evolution reaction, polarization curves were measured for undoped and the doped MoS_2 NCs. At the overpotential of $\eta = -300$ mV, the current densities, listed from greatest to least, are $FeMoS_2$, $CoMoS_2$, MoS_2, $NiMoS_2$, and $MnMoS_2$, and the order of catalytic activity found from Tafel slopes is $CoMoS_2 > MoS_2 > NiMoS_2 > FeMoS_2 > MnMoS_2$. The increasing number of catalytically active sites in Co doped MoS_2 NCs might be responsible for their superior electrocatalytic activity. The present results show that the magnetic order-disorder behavior and catalytic activity can be modulated by choosing the suitable dopants in NCs of 2D materials. *Published by AIP Publishing.* https://doi.org/10.1063/1.5043208

I. INTRODUCTION

Two-dimensional (2D) transition metal dichalcogenides (TMDs) are a class of materials with the formula MX_2, where M is a transition metal element (Mo, W, etc.) and X is a chalcogen (S, Se, or Te). 2D TMDs form layered structures in the form X–M–X, with the chalcogen atoms in two hexagonal planes separated by a plane of metal atoms. The layer-dependent properties of nanoscale TMDs have recently attracted a great deal of attention due to their extraordinary electrocatalytic, biomedical, and optoelectronic properties.[1–10] Unlike other 2D materials, such as graphene, these materials are semiconductors with tunable (1.3–1.8 eV) band gaps.

Recent observation[11–13] of intrinsic 2D ferromagnetism in monolayer van der Waals crystals such as CrI_3, $Cr_2Ge_2Te_6$, and VS_2 has invigorated the field of low-dimensional magnetism in layered compounds. The above 2D materials intrinsically contain magnetic elements such as Cr and V, which give rise to ferromagnetic behavior. In particular, there have been numerous theoretical works that have appeared[14–30] in realizing the dilute 2D semiconducting materials for next generation spintronic materials, which do not contain magnetic elements intrinsically, followed by promising experimental observations.[31–37] For instance, Yan *et al.* have shown[32] that upon Li intercalation the crystal structure transformed from 2H to 1 T phase and the magnetism was significantly enhanced from diamagnetism to paramagnetism in 2H-MoS_2 nanostructures. With further annealing in argon atmosphere the 2H phase recovered gradually from 1 T phase and the magnetism decreased correspondingly, attributed to the Mo atoms of 1T-MoS_2. In another work,[31] freestanding MoS_2 nanosheets reveal the clear room-temperature ferromagnetism for all the MoS_2 nanosheets. Furthermore, results indicate that the saturation magnetization of the nanosheets increase as the size decreases, attributed to the presence of edge spins on the edges of the nanosheets. Cao *et al.* have shown[33] vacancy induced ferromagnetism in MoS_2 nanosheets. Huo *et al.* reported[36] that multilayer WS_2 nanosheets exhibit strong ferromagnetic behavior with saturation magnetization (M_S) of 0.0058 emu/g and coercive field (H_C) of 92 Oe at room temperature, attributed to the zigzag edge sulfur and tungsten atoms. In addition, a few more reports have recently appeared[34,35,37] on the magnetic properties of TMD nanostructures upon doping with Co, and Mn prepared through the hydrothermal method. However, to date, the experimental studies on the magnetic properties of TMD nanostructures are limited. Most of the prior works focused on the magnetic properties mainly at the low (<5%–7%) doping level, and the relevance to their catalytic activity is not studied. To broaden the current knowledge and understanding on the doping induced magnetic properties, a comprehensive experimental study is required—that forms the first part of this study.

TMD NCs are also known to show excellent catalytic properties.[38–44] For instance, MoS_2 is a potential hydrogen

[a)]L. M. Martinez and J. A. Delgado contributed equally to this work.
[b)]srao@utep.edu

evolution material for clean energy applications. The evolution of hydrogen from water has allured the scientific community for the possibility of using hydrogen as a clean energy source. In the process of extracting hydrogen from water via hydrogen evolution reaction (HER), studies[45–49] have shown that Pt electrodes possess the best electrocatalytic properties. If it were not for the rarity of this element, the pursuit of other materials for the reaction would not be necessary. It is therefore in the best interest of the scientific community to find earth-abundant materials that can be used in place of Pt. One such earth-abundant material is MoS_2, which, in its bulk form, has been suggested for use as a catalyst in the evolution of hydrogen. MoS_2 was originally studied as a catalyst for hydrodesulfurization.[50–53] It has been shown[38–44] that the electrocatalytic performance of MoS_2 can be improved when it is prepared in the nanocrystalline form due to the formation of increasing number of active edge sites by doping with transition metals, in the same way as was done for hydrodesulfurization. In the second part of this paper, the catalytic properties of the transition metal (Co, Ni, Fe, and Mn) doped (10%) MoS_2 NCs were studied.

Together, in this work, transition metal (Co, Ni, Fe, Mn) (10%) doped MoS_2 NCs were prepared and their magnetic and catalytic properties were studied. In particular, it has been shown that it is possible to induce room temperature weak ferromagnetism in Co, Ni, and Fe doped MoS_2 NCs, while Mn doped MoS_2 NCs showed paramagnetic-like behavior at room temperature. Furthermore, the catalytic performance of doped materials is compared with respect to that of pure MoS_2 NCs. This study forms a significant step forward to introduce new opportunities for fully exploiting these materials for advanced spintronic and catalytic applications.

II. EXPERIMENTAL DETAILS

MoS_2 NCs were synthesized by using a most common facile bottom-up "hydrothermal method". Unlike other "top-down" approaches (chemical exfoliation, sonication of bulk MoS_2, electro-Fenton processing, etc.), this route eliminates harsh synthesis conditions, excludes hazardous chemicals, and is faster. Hydrothermal method has been routinely employed[35,37,54,55] in preparing the nanostructures of transition metal (Co, Cu, V, Mn) doped MoS_2 up to the doping level of 16%. Previously, this method was successfully employed[56–58] by some of us (Singamaneni and Gandha) in preparing nanocrystalline magnetic nanowires. To describe the procedure briefly,[59,60] 0.4 g of Na_2MoO_4-$2H_2O$ was dissolved in 30 ml distilled water under sonication for 20 min. At this step, the desired metal precursor is added. 0.38 g of dibenzyl disulfide was then added to the solution along with 30 mL of ethanol and sonicated for 30 min. The solution was then transferred into a 100 ml Teflon-lined stainless-steel autoclave and was maintained at 250 °C for 18 h. After 18 h, the reaction system was allowed to cool down to ambient temperature. The obtained products were collected by centrifugation and washed with deionized water. The stoichiometric MoS_2 NCs were filtered and left to dry over night at room temperature in vacuum. Using this approach, 10% Co, Ni, Fe, and Mn doped MoS_2 NCs were prepared. All the precursors were purchased from Alfa Aeser and used without further purification. The magnetization measurements were performed using Quantum Design PPMS (5–300 K, ±5 T). Electron spin resonance (ESR) data were recorded on a Bruker EMX Plus X-band (~9.40 GHz) ESR spectrometer, equipped with a high sensitivity probe head. A ColdEdge™ ER 4112HV In-Cavity Cryo-Free VT system connected with an Oxford temperature controller was used for low temperature measurements. The complete system was operated by Bruker Xenon software. Additionally, all ESR experimental settings were kept constant for reproducibility. For all ESR measurements, the sample was wrapped in a Teflon tape, and inserted into a quartz tube. During the magnetic measurements, all the samples were carefully handled with nonmagnetic capsules and tapes to avoid contamination. X-ray diffraction (XRD), transmission electron microscopy (TEM), Raman spectroscopy, and X-ray photo absorption spectroscopy (XPS) measurements were employed to study the crystallinity, phase formation, doping effects, and valence states of elements before and after doping with transition metal elements (data not shown).

All catalysts were accessed heterogeneously for hydrogen production. Prior to electrochemical studies, the catalysts were deposited on a conductive fluorinated-tin oxide (FTO) substrate,[61] with a conductive adhesive silver paste to better support the catalyst. FTO glass was cleaned by being sonicated in acetone, isopropyl alcohol, and deionized water separately. The silver paste was then coated on top of the active side of the FTO with an area of 0.25 cm^2 (0.5 cm × 0.5 cm). 0.5 mg of the catalyst was dispersed in 1 ml ethanol and sonicated for 30 min to form a homogeneous ink. 10 μl of the catalyst ink was then drop cast on the silver paste and the plate was allowed to dry in ambience, which was later used as the working electrode for electrochemical measurements.

All electrochemical studies were performed on a CHI760D potentiostat[61] with a three-electrode electrochemical cell in room temperature. A platinum wire was utilized as the counter electrode while a saturated calomel electrode (SCE) was used as the reference electrode. All potentials displayed in this work were referred to reversible hydrogen electrode (RHE) by adding a value of $(0.245 + 0.059\,pH)$ to the data obtained using a SCE reference electrode. An aqueous solution of 0.5M H_2SO_4 was used as both the proton source and electrolyte. The solution was saturated with nitrogen gas to remove the dissolved oxygen prior to each measurement. Electrical impedance spectroscopy (EIS) was obtained at different overpotentials from 100 KHz to 0.1 Hz with AC voltage of 5 mV.

III. RESULTS AND DISCUSSION

A. Magnetic properties

1. MoS_2 NCs

To study the magnetic properties of MoS_2 NCs, temperature- and magnetic field-dependent magnetization

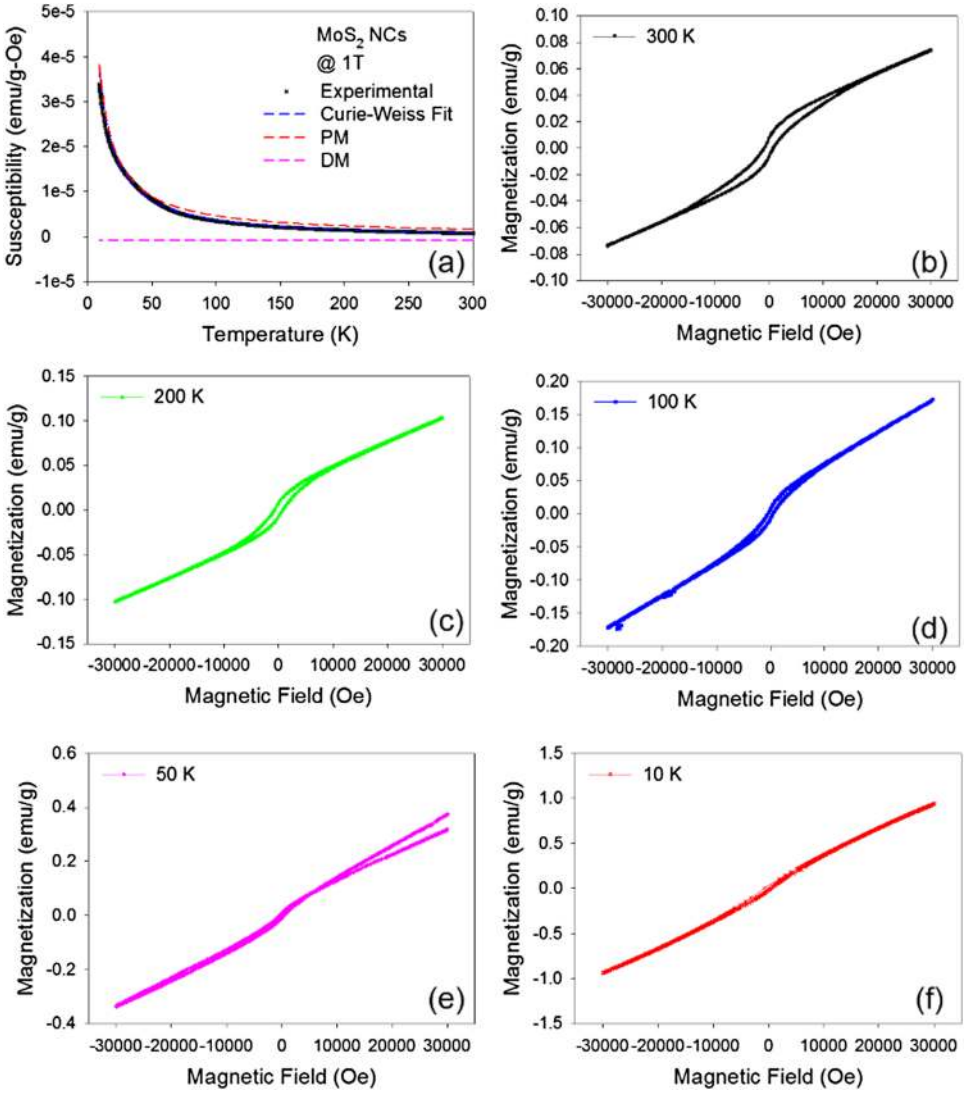

FIG. 1. The temperature-dependent magnetic susceptibility and magnetic field-dependent magnetic behavior of MoS_2 NCs. Fig. 1(a) also includes the applicability of the modified Curie-Weiss model.

measurements were performed. In Fig. 1(a), the temperature dependence of susceptibility (χ) is plotted. χ was measured from 10 to 300 K, after a $\mu_0 H = 1$ T magnetic field cooling. As it can be noticed, χ increased with cooling. A similar observation was reported on many other materials[31,32,37,62] such as exfoliated WS_2 nanosheets, graphene nanoribbons, Li intercalated MoS_2 nanosheets, and amorphous MoS_2.

To better understand the observed magnetic behavior, the χ-T curve was fitted using modified Curie-Weiss(CW) model[32] $\chi = \chi_{dm} + C/(T + \theta)$, which involves the diamagnetic and paramagnetic contributions. Here, χ_{dm} is the diamagnetic susceptibility, C = Curie constant, θ = CW temperature, and T = measurement temperature. The fitting results (blue) are shown in Fig. 1(a) along with the experimental data (black). Both the diamagnetic and paramagnetic components were resolved. In addition, the fitting results are tabulated in Table I. The value of θ was obtained as 3 K for the MoS_2 NCs. As shown in Table I, the value of θ is positive indicating antiferromagnetic behavior,[32] which, however, is associated with uncompensated spins that result in finite magnetization. That is the typical signature of canted antiferromagnetic phase. Negative θ values would indicate ferromagnetism.

Now, attention will be turned to the magnetic field-dependent magnetization behavior. Isothermal magnetization as a function of magnetic field was measured between 10 and 300 K. The data are plotted in Figs. 1(b)–1(f). At 10 K, observation of a nearly anhysteretic behavior with a positive slope indicates canted antiferromagnetic phase. As temperature increases further, a more magnetic hysteretic behavior was observed at low fields but the anhysteretic behavior persists at higher fields. These features together with χ-T variation [Fig. 1(a)] indicate that MoS_2 NCs showed a canted antiferromagnetism at low temperature and weak ferromagnetism at room temperature. It was verified that the modified

TABLE I. The parameters obtained from the modified Curie-Weiss (CW) fits of all the samples studied here.

Sample	C	Θ (K)	χ_{dm}
Undoped MoS_2 NCs	4.767×10^{-04}	3.406	-9.454×10^{-07}
Fe doped MoS_2 NCs	4.257×10^{-04}	3.296	-3.732×10^{-07}
Ni doped MoS_2 NCs	5.396×10^{-04}	3.173	-6.123×10^{-07}
Co doped MoS_2 NCs	9.895×10^{-04}	2.935	1.883×10^{-06}
Mn doped MoS_2 NCs	3.756×10^{-03}	2.841	-5.526×10^{-06}

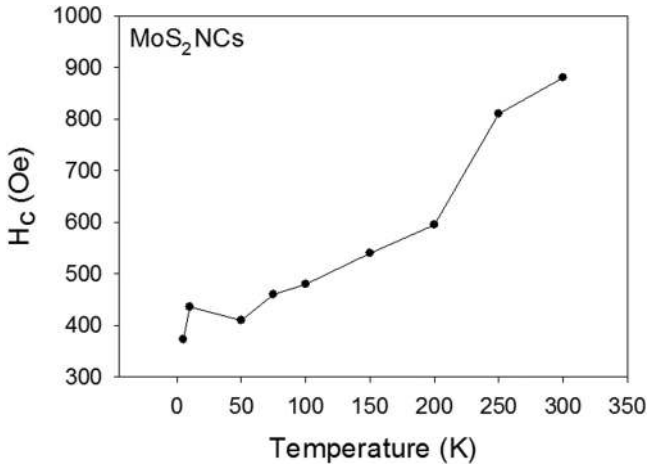

FIG. 2. The temperature variation of coercive field of MoS_2 NCs.

Brillouin function[32] (see below) could not account for the room temperature M-H behavior.

$$M = X_d H + Ms\left[\frac{2J+1}{2J}\coth\left(\frac{2J+1}{2J}X\right) - \frac{1}{2J}\coth\left(\frac{X}{2J}\right)\right].$$

This function consists of a linearly field-dependent function, which represents diamagnetism added with the classic Brillouin function, which refers to paramagnetism. In the above equation, the variable M_s is the saturated magnetization, $Ms = Ng\mu J$, where N is the density of spins, μ is Bohr's magneton, g is the Lande g-factor, and J is the angular momentum number. The variable X is equaled to $gJ\mu H/kT$, where k is Boltzmann's constant, and T is temperature. Fits for the data that were accumulated were obtained by using the modified Brillouin function; however, the numerical values of temperature in these fits did not correlate with what was seen in experimentation, verifying that the modified function could not account for the magnetic-field-dependent magnetization data that were observed at room temperature. A strong hysteretic behavior at 300 K, rather than at 10 K, was noticed. This observation is also reflected in the temperature-dependent coercive field (H_c) trend plotted in Fig. 2. It is also noticed that H_c increased from 373 to 880 Oe as the temperature increased from 10 to 300 K. This infers that the ferromagnetism observed at room temperature is of short-range.

To corroborate the magnetic data, the temperature-dependent (50–300 K) resistance measurements (data not

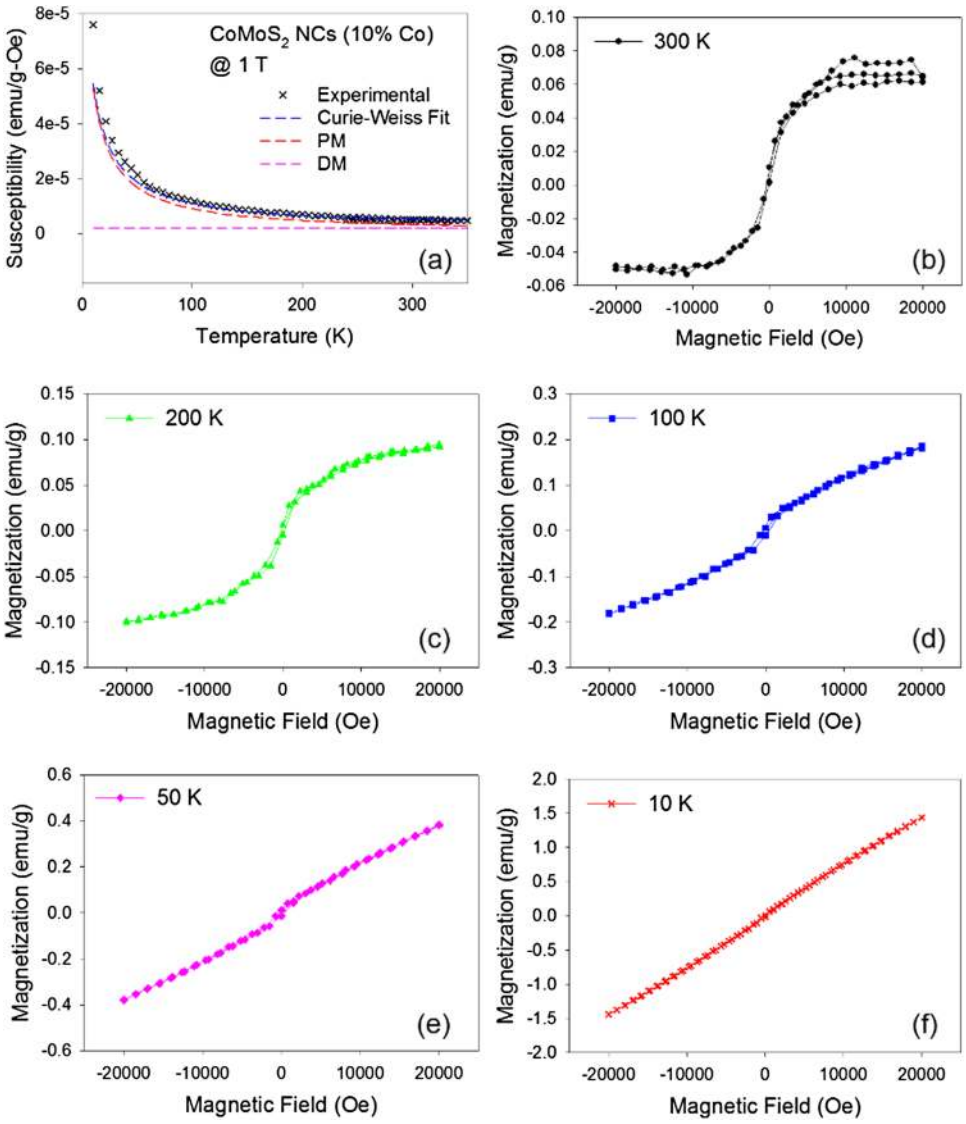

FIG. 3. The temperature-dependent magnetic susceptibility and magnetic field-dependent magnetic behavior of Co doped (10%) MoS_2 NCs. Fig. 3(a) also shows the applicability of the modified Curie-Weiss model.

shown) were performed on all the materials studied here, including undoped MoS_2 NCs. The data showed semiconducting behavior (resistance increases as the sample is cooled), consistent with the literature reports,[63] and revealed very little (<0.5%) magnetic field dependence of resistance even upon the application of 3 T magnetic field. These observations are the typical signatures of canted antiferromagnetism.

To provide additional information on the presence of magnetic moments, in our previous work,[59,60] using X-band (~9.43 GHz) ESR spectroscopy performed on MoS_2 NCs, our group has reported several electron spin centers such as oxygen species, sulfur vacancies, thio-, and oxo-Mo^{5+}. It is believed that the exchange interaction among these magnetic species could lead to the observed magnetic phases. These measurements coupled with the data obtained from XPS and Raman spectroscopy showed no indication of unwanted extrinsic impurities that could account for the magnetic behavior observed in the present work.

2. Co doped MoS_2 NCs

The temperature-dependent magnetic susceptibility (χ) data were obtained after the sample was cooled to 10 K in $\mu_0 H = 1$ T magnetic field [see Fig. 3(a)]. The magnetization value (0.8 emu/g) observed in the present study is higher than those (0.006 to 0.3 emu/g) reported[35,37,54,55] in the literature on similar systems such as Co, Cu, and V doped (<7% doping) MoS_2 nanostructures prepared through hydrothermal method. As displayed in Fig. 3(a), the temperature dependence of magnetic susceptibility can be well described by the modified CW model. A positive θ of 3 K (see Table I) was obtained, which indicates that the material is antiferromagnetic below the temperature of 3 K.

Isothermal magnetization measurements were performed on Co doped MoS_2 NCs by sweeping the magnetic field from −2 to +2 T at 10, 50, 10, 200, and 300 K. The data are presented in Figs. 3(b)–3(e). At 10 K, magnetization shows anhysteretic behavior with the magnetic field with the positive slope, which indicates the (canted) antiferromagnetic behavior. Interestingly, with further increase in temperature, a more hysteretic behavior with coercive field of 400 Oe becomes pronounced, suggesting unambiguous room-temperature ferromagnetism, as evidenced from the s-shaped hysteresis loop. In addition, the applicability of the Brillouin function was tested, and found that it could not account for the magnetic-field-dependent magnetization data observed at

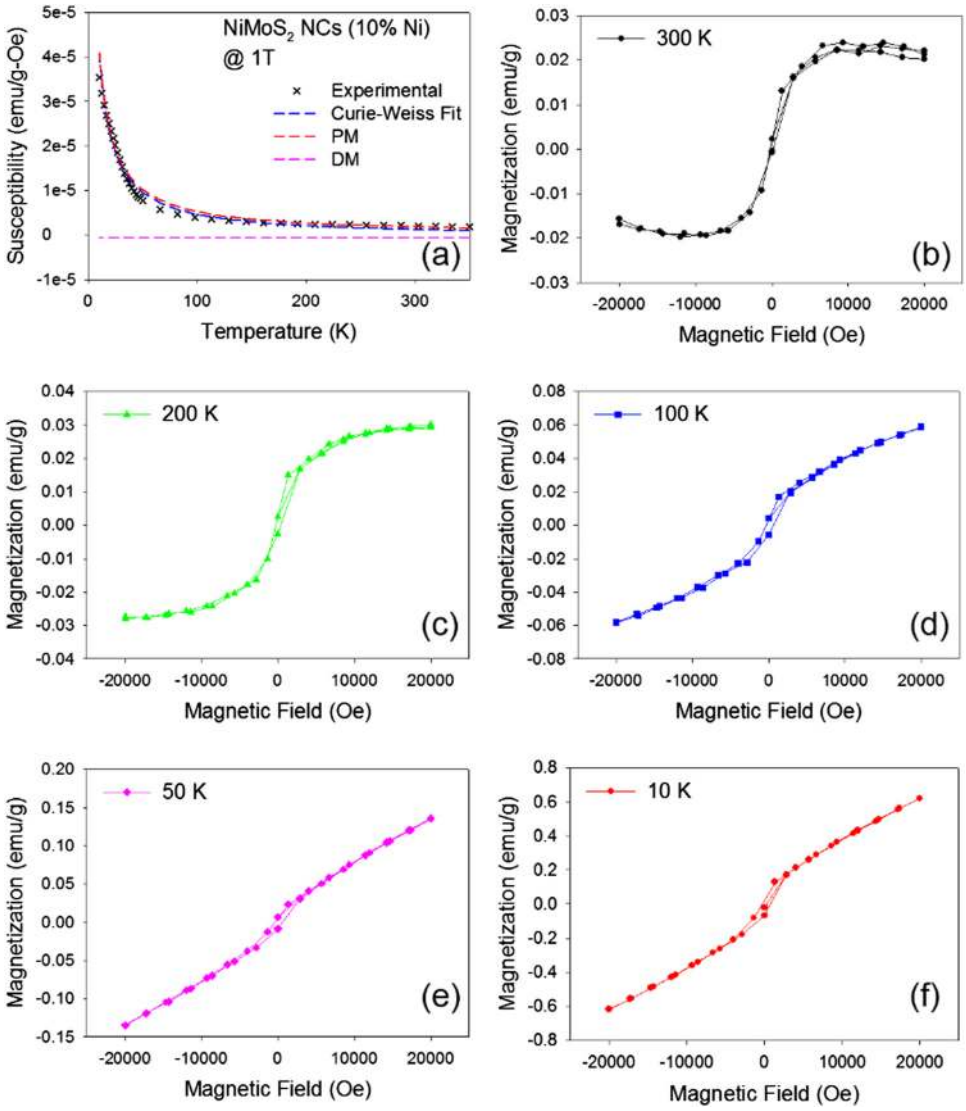

FIG. 4. The temperature-dependent magnetic susceptibility and magnetic field-dependent magnetic behavior of Ni doped (10%) MoS_2 NCs. Fig. 4(a) also shows the applicability of the modified Curie-Weiss model.

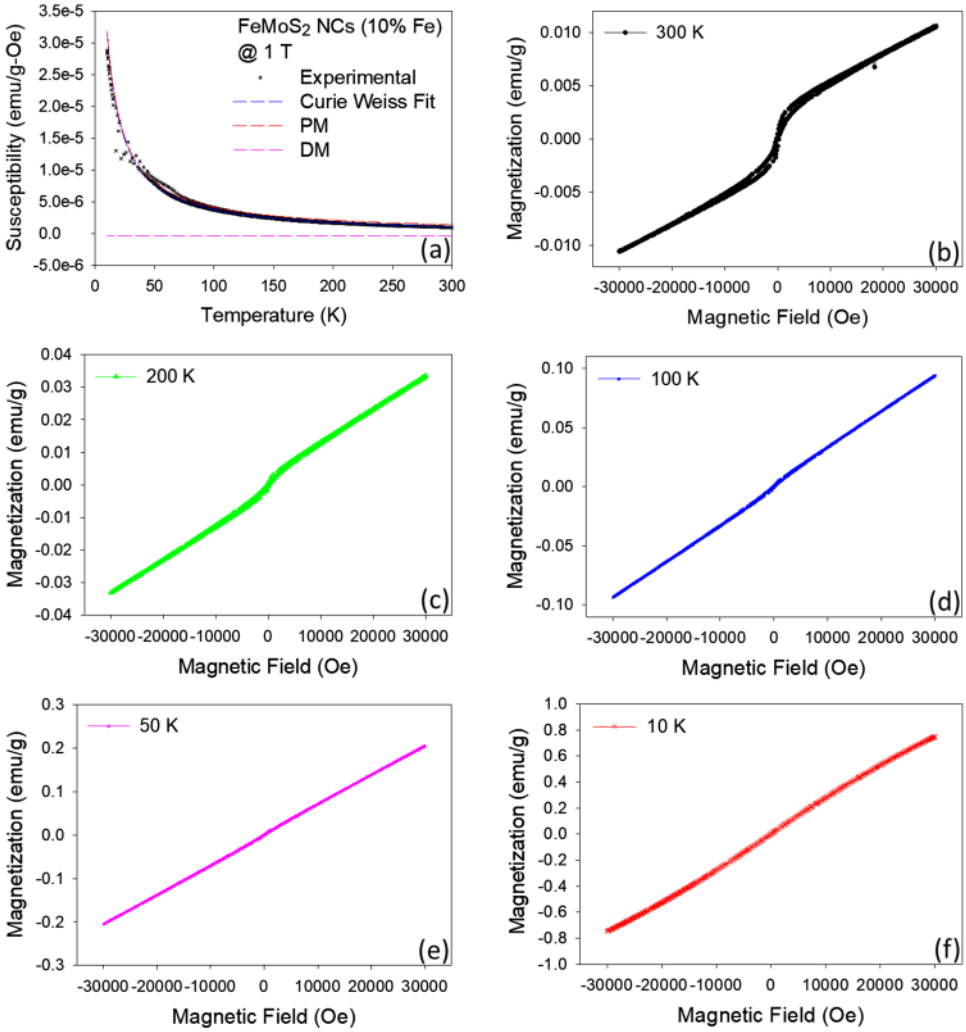

FIG. 5. The temperature-dependent magnetic susceptibility and magnetic field-dependent magnetic behavior of Fe doped (10%) MoS_2 NCs. Fig. 5(a) also shows the applicability of the modified Curie-Weiss model.

room temperature. The saturation magnetization (magnetization at the maximum applied magnetic field) decreases as the measurement temperature increases from 10 to 300 K. This trend is consistent with the temperature-dependent magnetic susceptibility data as shown in Fig. 3(a). Xiang *et al.* have also reported[35] room temperature ferromagnetism from Co doped (<7%) MoS_2 nanosheets.

XRD patterns (data not shown) obtained on the samples studied here are identical to the ones reported on the best samples prepared through hydrothermal method in the literature,[31,35,37,64] thus confirming that there is no or minimal segregation/clustering of dopants. If there is a significant clustering effect, one would expect to observe high ferromagnetic T_C much beyond room temperature,[65] which is clearly not the case here.

3. Ni doped MoS_2 NCs

Temperature-dependent magnetic susceptibility data was collected after the sample was field cooled at $\mu_0 H = 1$ T magnetic field [Fig. 4(a)]. The magnetization value (0.4 emu/g) observed in the present study is comparable to those reported in the literature on similar systems.[35,37,54,55] The modified CW model as depicted in Fig. 4(a) can describe the temperature-dependent magnetization behavior. The obtained θ is 3 K (see Table I), suggesting that the material is antiferromagnetic below 3 K.

The isothermal magnetization measurements were performed on Ni doped MoS_2 NCs by sweeping the magnetic field from −2 to +2 T at 10, 50, 10, 200, and 300 K. The data are presented in Figs. 4(b)–4(e). At 10 K, magnetization anhysteretic behavior as a function of magnetic field was observed, which indicates (canted) antiferromagnetic behavior. Interestingly, as temperature is increased further, a hysteretic behavior with coercive field of 175 Oe appears, suggesting unambiguous room-temperature ferromagnetism. The saturation magnetization decreases as the measurement temperature increased from 10–300 K. This trend is consistent with the temperature-dependent magnetic susceptibility data shown in Fig. 4(a). Similar to the case of Co doped MoS_2 NCs, Brillouin function could not account for the magnetic-field-dependent magnetization data observed at room temperature. To our knowledge, with the exception of one report[66] on the catalytic behavior of Ni doped MoS_2 nanoparticles, there have been no previous works reporting on the magnetic properties of Ni doped MoS_2 NCs to compare these data at any doping percentage.

4. Fe doped MoS_2 NCs

Like the measurements performed on Co and Ni doped MoS_2 NCs, magnetization data were collected on Fe doped MoS_2 NCs. The temperature-dependent magnetic susceptibility

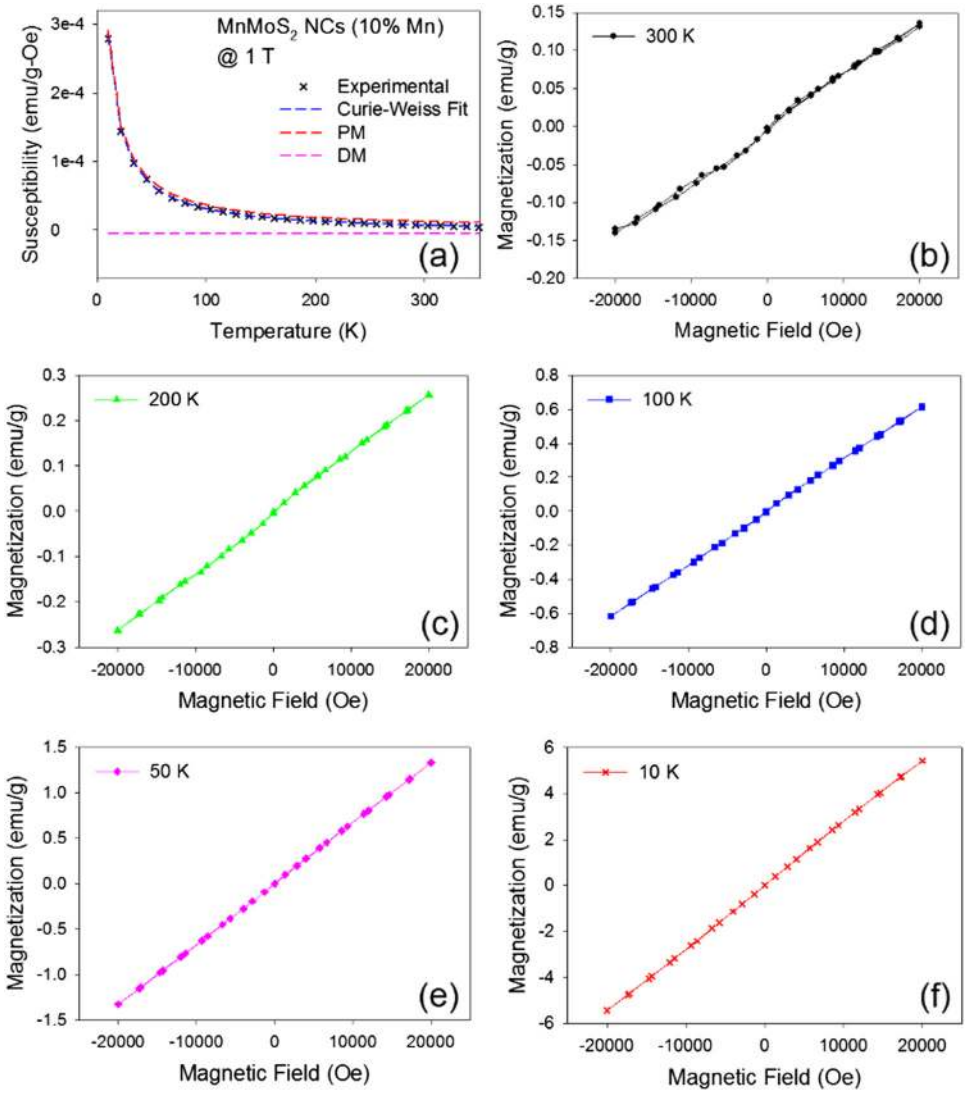

FIG. 6. The temperature-dependent magnetic susceptibility and magnetic field-dependent magnetic behavior of Mn doped (10%) MoS_2 NCs. Fig. 6(a) also shows the applicability of the modified Curie-Weiss model.

data were recorded after the sample was cooled in $\mu_0 H = 1$ T magnetic field [see Fig. 5(a)]. The magnetization value (0.3 emu/g) obtained in the present study from the χ-T curve is comparable to that (0.25 emu/g) reported in the literature on 1.74% Fe doping in MoS_2 nanostructures.[64] As displayed in Fig. 5(a), it was found that the modified CW model describes well the temperature-dependent magnetic susceptibility behavior. From the fits, the θ is obtained as 3 K (see Table I), which indicates that the material is antiferromagnetic below 3 K.

The isothermal magnetization data are presented in Figs. 5(b)–5(e). At 10 K, similar to the previous samples, magnetization shows anhysteretic behavior with the magnetic field, which indicates (canted) antiferromagnetic behavior. However, at 300 K, the M-H behavior of this material shows a combination of ferromagnetic (at low fields) and antiferromagnetic behavior (at high fields). This is in sharp contrast with the Co and Ni doped samples, which show complete ferromagnetic behavior at room temperature. The saturation magnetization decreases as the measurement temperature increased from 10 to 300 K. This trend is consistent with the temperature-dependent magnetic susceptibility data shown in Fig. 5(a). In addition, it has been verified that Brillouin function could not account for the magnetic-field dependent magnetization data observed at 300 K. Xia *et al.* also reported[64] room temperature ferromagnetism in Fe doped (<3.18%) MoS_2 nanosheets prepared through hydrothermal process. The interaction between the sulfur vacancies and the dopants is argued to be at play. A similar situation may be expected to happen in the present case as well.

5. Mn doped MoS_2 NCs

Temperature-dependent magnetic susceptibility and magnetic field-dependent magnetization measurements were performed on Mn doped MoS_2 NCs. As shown in Fig. 6(a), the magnetic susceptibility increased as the sample temperature is lowered from 300 K to 10 K. More importantly, it was noticed that the magnetization (measured at 10 K, 1 T) is about 6 times higher than that of pure MoS_2 NCs [see Fig. 1(a)]. This observation is the direct effect of doping with Mn. To gain additional insights into the magnetism, the χ-T curve was fitted to the modified CW model comprising both diamagnetic and paramagnetic contributions. The highest Curie constant of 4×10^{-3} obtained from the χ-T curve fitting signifies the larger magnetization in comparison to the

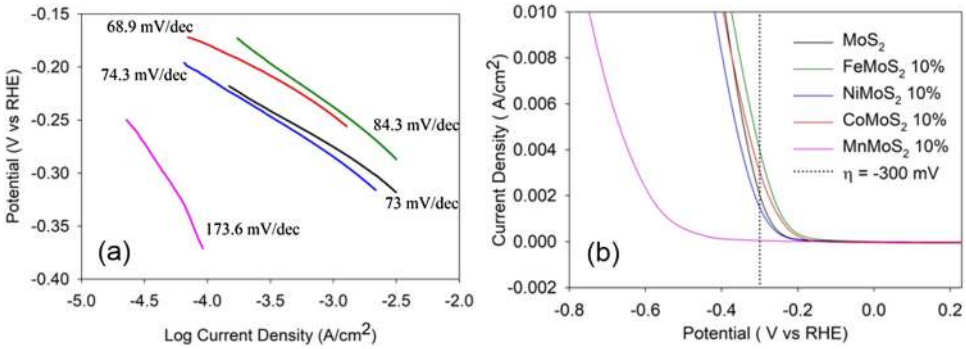

FIG. 7. (a) Tafel plots of pristine and 10% doped (Co, Ni, Fe, and Mn) MoS_2 NCs and (b) and polarization curves of pristine and TM doped MoS_2.

materials discussed above. The fitting results are shown in Fig. 6(a) along with the experimental data. Using this model, the diamagnetic and paramagnetic components were resolved and the CW constant (θ) as 3 K (see Table I) was obtained, which indicates that the material is antiferromagnetic below 3 K. However, a much weaker ferromagnetism was observed at 300 K as reflected from the hysteretic behavior at low fields, and a predominant paramagnetic nature was observed at higher fields. A similar weak ferromagnetism was previously reported[67] for Mn doped SnSe alloys prepared via molecular beam epitaxy methods. Wang *et al.* reported[37] room temperature ferromagnetism in Mn doped (7%) MoS_2 NCs. Park *et al.* have reported[68] a similar room temperature ferromagnetism from MoS_2 NCs upon doping with MnO_2 by electrochemical method, associated with the saturation magnetization of 0.02 emu/g. This work not only shows that magnetic properties strongly depend on the nature of the dopant but also the magnetic order-disorder transition varies with dopant type such that Co and Ni doping produces stronger ferromagnetic behavior than Fe and Mn at least at 300 K.

B. Electrocatalytic properties

It has been shown that the electrocatalyic performance of MoS_2 NCs can be engineered by doping the active edge sites with transition metals. To study the HER performance, polarization curves (see Fig. 7) were obtained for pristine MoS_2 NCs as well as the doped samples. At an overpotential (η) of 300 mV, the current densities for MoS_2, $CoMoS_2$, $NiMoS_2$, $FeMoS_2$, and $MnMoS_2$ were found to be 2.09, 3.00, 1.5, 4.05 mA/cm^{-2}, and 52 $\mu A/cm^{-2}$. Listed from greatest to least for comparison, the reaction kinetics are as follows: $FeMoS_2 > CoMoS_2 > MoS_2 > NiMoS_2 > MnMoS_2$; this was observed to be true for $-372.8\,mV \leq \eta \leq -169.6\,mV$. This progression is the exact same order of activity that was previously found by calculating the hydrogen absorption free energy (ΔG_H).[69] Wang *et al.* and other groups have doped different transition metals to MoS_2 nanostructures, similar to the metals used in the experiments presented here and observed current densities that are comparable with data collected for this study.[69,70] The onset potential for the MoS_2 NCs presented here was 141 mV; this is comparable to the work done by Ren.[71] Thus, the present observations are consistent with the literature reports.

For the HER, the Tafel slope and exchange current density can provide information about the reaction mechanism and kinetics of the process. The Tafel slopes also indicate the rate-limiting step in the HER.[72] Essentially, the lower the Tafel slope, the faster the reaction takes place, and the faster hydrogen is produced. Doping with different transition metals showed a slight change in the Tafel slope, which is consistent with other literature reports.[43,66,69,73]

EIS was performed on the samples at overpotentials of 0.445, 0.5, 0.545, and 0.645 V. Figure 8 shows the EIS measurements taken at $\eta = 0.5$ V. Smaller semicircle diameters correspond to higher charge transfer, higher conductivity, and thus lower charge transfer resistance (R_{ct}). The samples can be ranked in the order from least to greatest R_{ct} in the following order: Fe, Co, pristine MoS_2, Ni, Mn. Fe doped MoS_2 NCs have the greatest conductivity and charge transfer ability, while Mn doped MoS_2 NCs have the least. Another literature report performed a similar electrocatalytic study of TM-doped MoS_2 and found the exact same progression,[69] with R_{ct} increasing from Fe to Ni doping in the same order. This study [Fig. 8(b)] of Mn doped MoS_2 showed poor HER performance.

The electrocatalytic performance of $CoMoS_2$ NCs was examined using chronoamperometry to determine the long-term stability of the NCs. The chronoamperometric studies were operated in a custom-built two-compartment gas-tight

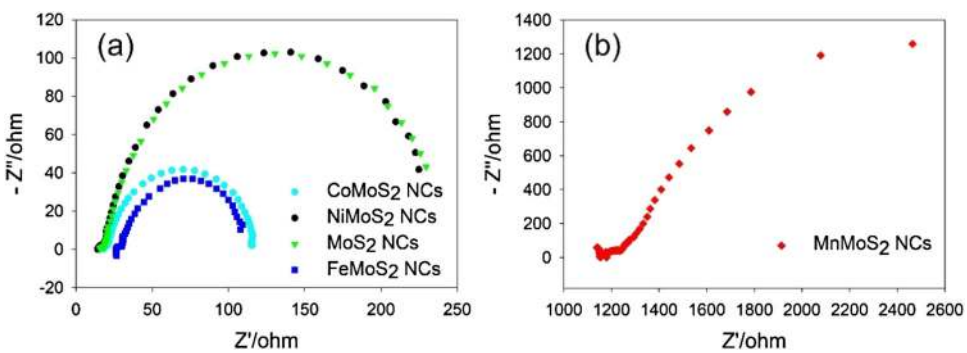

FIG. 8. (a) EIS plots for Co, Ni, Fe doped MoS_2 NCs, and pristine MoS_2 NCs; $\eta = 0.5$ V. (b) EIS plot for Mn doped MoS_2 NCs; $\eta = 0.5$ V.

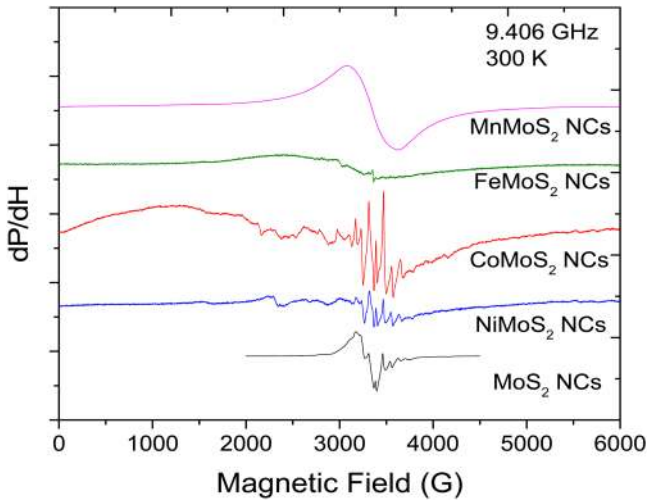

FIG. 9. X-band room temperature (300 K) ESR spectra collected from MoS_2, Co, Ni, Fe, and Mn doped MoS_2 NCs.

electrochemical cell under an argon atmosphere. One of the compartment of the cell contains the working electrode and the reference electrode while the other compartment contains the counter electrode. The solution (0.5M H_2SO_4 in water) was saturated with argon gas prior to the measurement and the solution on the side of the cell containing the working electrode was kept stirring to remove the *in situ* generated hydrogen gas. The experiment was conducted with an initial current density of 10 mA/cm^2 along with a constant overpotential of $\eta = 850$ mV. The current density was observed to stabilize after approximately 5 h. Even after over 23 h of operation, the $CoMoS_2$ NCs were seen to be electrocatalytically active. Thus, the stability of the nanocrystals has been demonstrated through pragmatic means.

Interestingly, the electrochemical behavior shown in this work is in agreement with what is known in the literature.[69,74,75] As noted above, the electrocatalytic activity, from greatest to least is: $FeMoS_2 > CoMoS_2 > MoS_2 > NiMoS_2 > MnMoS_2$, which is consistent with previous works.[69,74,75] Since the adsorbed atomic hydrogen Gibbs free energy (ΔG_H) is the key to the HER electrocatalytic activity of a catalyst, ΔG_H closer to zero corresponds to higher activity. Incorporation of transition metals to MoS_2 does not affect the ΔG_H of the Mo-edge, but lowers the ΔG_H of S-edge, which makes the catalytic inert S-edge catalytically active. Previous studies[69,74,75] have shown similar effects when doping with Fe and Co, leading to ΔG_H value closer to zero in the S-edge of MoS_2, which explains why these two catalysts exhibit the best efficiency.

Now, why the variations in the magnetic and catalytic properties occur as a function of transition metal doping is discussed. The present work, as well as earlier reports[76–79] showed that the transition metal elements show interesting magnetic properties as well as pronounced catalytic activity. From the current observations, it is learned that the Mn doped MoS_2 NCs showed least catalytic performance and showed predominant paramagnetism at room temperature. Whereas the pristine MoS_2 and Co, Ni, and Fe doped MoS_2 NCs showed good catalytic performance, as well as stronger room temperature ferromagnetism. To better understand the relationship between the magnetism and catalytic performance, X-band ESR measurements were performed on all the samples at room temperature (300 K). The data are presented in Fig. 9. As it can be clearly noticed, Mn doped MoS_2 NCs did not show signals coming from the catalytically active centers, except the strong signal that comes from Mn^{2+} only. On the other hand, the samples doped with Co, and Ni, including undoped MoS_2 NCs, showed many sharp ESR signals, indicating the presence of larger number of catalytically active centers. Hence, it is believed that Co doped MoS_2 NCs showed superior catalytic performance compared to Mn doped MoS_2 NCs. These active defect centers contain unpaired electron spins due to uncoordinated and dangling bonds. The observed ferromagnetic behavior could have resulted from the interaction between these active spin centers.

Furthermore, the morphology of 10% Co doped MoS_2 NCs is distinctly different from that of 10% Mn doped MoS_2 NCs, as reflected from the TEM bright field images displayed in Fig. 10. The Co doped sample shows a flowery morphology with randomly oriented sheets of MoS_2 that are only a few monolayers thick as indicated by the selected area diffraction (SAED) pattern shown as the inset of Fig. 10(a). On the other hand, the Mn doped MoS_2 showed a mixed morphology with some flowery structures, but also mixed with many faceted plates of well crystallized MoS_2 that are several hundred nanometers wide and the corresponding SAED pattern is shown as the inset of Fig. 10(b). The [111] zone axis SAED pattern indicates single crystalline nature of these plates with six fold symmetry. One would expect the flowery morphology of Co doped samples to have more surface area compared to the Mn doped samples, which would explain the high catalytic activity of these samples.

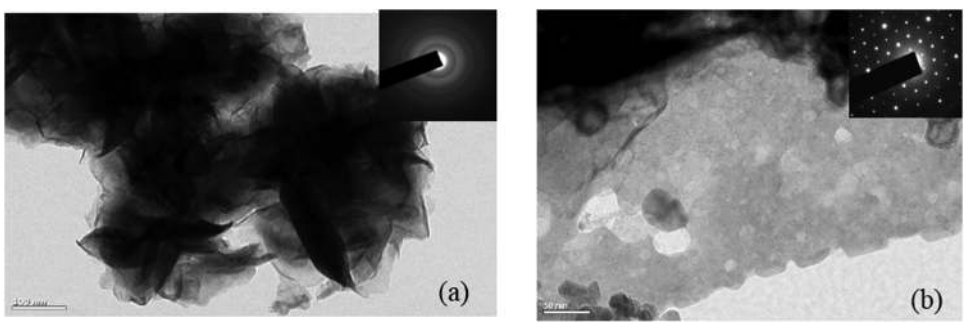

FIG. 10. Bright field transmission electron microscopic image of 10% Co doped MoS_2 (a) and 10% Mn doped MoS_2 nanocrystals (b) and the insets are the SAED patterns for both Co and Mn doped MoS_2 NCs, respectively.

IV. CONCLUSIONS

To conclude, the magnetic and catalytic properties of hydrothermally grown transition metal doped (10% of Co, Ni, Fe, and Mn) MoS_2 NCs associated with a particle size of 25–30 nm have been reported. Interestingly, the undoped MoS_2 NCs showed a mixture of canted anti-ferromagnetic and ferromagnetic behavior. MoS_2 NCs doped with Co, Ni, and Fe exhibited profound room temperature ferromagnetism. On the other hand, Mn doped MoS_2 NCs showed room temperature paramagnetic nature, predominantly. For all the materials, modified CW law described the temperature dependent magnetic behavior, and the ground state is canted antiferromagnetic phase associated with uncompensated electron spins. In addition, the hydrogen evolution reaction performance was also studied. The present study compared the current densities (j), measured at the overpotential of $-372.8\,\text{mV} \leq \eta \leq -169.6\,\text{mV}$, listed from greatest to least, $j(FeMoS_2) = 4.05$, $j(CoMoS_2) = 3.00$, $j(MoS_2) = 2.09$, $j(NiMoS_2) = 1.5$ mA/cm^2, and $j(MnMoS_2) = 52\,\mu\text{A/cm}^2$. The order of overall reaction activity is obtained from Tafel slopes as $CoMoS_2 > MoS_2 > NiMoS_2 > FeMoS_2 > MnMoS_2$. The electrochemical impedance spectroscopic measurements indicated that Fe doped MoS_2 NCs have the best conductivity and charge transfer ability, while Mn-doped MoS_2 NCs have the lowest. Co doped MoS_2 NCs show best catalytic activity when compared to Mn doped MoS_2 NCs. Most likely, it is due to the creation of a higher number of catalytically active centers in Co doped MoS_2 NCs compared to Mn doped MoS_2 NCs, as evidenced from room temperature ESR measurements.

ACKNOWLEDGMENTS

L.M.M., J.A.D., C.L.S., A.C., and S.R.S. acknowledge support from a UTEP Start-up Grant. L.M.M. acknowledges the Wiemer Family for awarding Student Endowment for Excellence. L.M.M, J.A.D, A.C, and S.R.S. acknowledge the NSF-PREM Program (DMR—1205302). L.M.M. acknowledges the NSF-LSAMP Ph.D. fellowship. This paper was prepared by Dr. Singamaneni and co-authors under the Award No. 31310018M0019 from The University of Texas at El Paso (UTEP), Nuclear Regulatory Commission. The Statements, findings, conclusions, and recommendations are those of the author(s) and do not necessarily reflect the view of the (UTEP) or The US Nuclear Regulatory Commission. Authors thank S. R. J. Hennadige for his help in ESR measurements. Work at Ames Laboratory by I.C.N. and K.G. was supported by the Critical Materials Institute, an Energy Innovation Hub funded by the U.S. Department of Energy, Office of Energy Efficiency and Renewable Energy, Advanced Manufacturing Office. Work at Ames Laboratory, operated by Iowa State University, was performed under Contract No. DE-AC02-07CH11358.

[1]Q. H. Wang, K. K-Zadeh, A. Kis, J. N. Coleman, and M. S. Strano, "Electronics and optoelectronics of two-dimensional transition metal dichalcogenides," Nat. Nanotechnol. **7**, 699 (2012).
[2]G. R. Bhimanapati, Z. Lin *et al.*, "Recent advances in two-dimensional materials beyond Graphene," ACS Nano **12**, 11509 (2015).
[3]S. Z. Butler, S. M. Hollen, *et al.*, "Progress, challenges, and opportunities in two-dimensional materials beyond graphene," ACS Nano **12**, 2898 (2013).
[4]Z. Lin, B. R. Carvalho, E. Kahn, R. Lv, R. Rao, H. Terrones, M. A. Pimenta, and M. Terrones, "Defect engineering of two-dimensional transition metal dichalcogenides," 2D Mater. **3**, 022002 (2016).
[5]H. I. Rasool, C. Ophus, and A. Zettl, "Atomic defects in two dimensional materials," Adv. Mater. **27**, 5771 (2015).
[6]J. Hong, Z. Hu, M. Probert, K. Li, D. Lv, X. Yang, L. Gu, N. Mao, Q. Feng, L. Xie, J. Zhang, D. Wu, Z. Zhang, C. Jin, W. Ji, X. Zhang, J. Yuan, and Ze Zhang, "Exploring atomic defects in molybdenum disulphide monolayers," **6**, 6293.
[7]A. Azizi, X. Zou, P. Ercius, Z. Zhang, A. L. Elı´as, N. Perea-López, G. Stone, M. Terrones, B. I. Yakobson, and N. Alem, "Dislocation motion and grain boundary migration in two-dimensional tungsten disulphide," Nat. Commun. **5**, 4867 (2014).
[8]X.-X. Li, Z.-Q. Fan, P.-Z. Liu, M.-L. Chen, X. Liu, C.-K. Jia, D.-M. Sun, X.-W. Jiang, Z. Han, V. Bouchiat, J.-J. Guo, J.-H. Chen, and Z.-D. Zhang, "Gate-controlled reversible rectifying behaviour in tunnel contacted atomically-thin MoS_2 transistor," Nat. Commun. **8**, 970 (2017).
[9]R. Kurapati, K. Kostarelos, M. Prato, and A. Bianco, "Biomedical uses for 2D materials beyond graphene: current advances and challenges ahead," Adv. Mater. **28**, 6052 (2016).
[10]Y. Sun, R. Wang, and K. Liu, "Substrate induced changes in atomically thin 2-dimensional semiconductors: Fundamentals, engineering, and applications," Appl. Phys. Rev. **4**, 011301 (2017).
[11]B. Huang, G. Clark, E. Navarro-Moratalla, D. R. Klein, R. Cheng, K. L. Seyler, D. Zhong, E. Schmidgall, M. A. McGuire, D. H. Cobden, D. X. Wang Yao, P. Jarillo-Herrero, and X. Xu, "Layer-dependent ferromagnetism in a van der Waals crystal down to the monolayer limit," Nature **546**, 270 (2017).
[12]C. Gong, L. Li, Z. Li, H. Ji, A. Stern, Y. Xia, T. Cao, W. Bao, C. Wang, Y. Wang, Z. Q. Qiu, R. J. Cava, S. G. Louie, J. Xia, and X. Zhang, "Discovery of intrinsic ferromagnetism in two-dimensional van der Waals crystals," Nature **546**, 265 (2017).
[13]M. Bonilla, S. Kolekar, Y. Ma, H. C. Diaz, V. Kalappattil, R. Das, T. Eggers, H. R. Gutierrez, M.-H. Phan, and M. Batzill, "Strong room-temperature ferromagnetism in VSe_2 monolayers on van der Waals substrates," Nat. Nanotechnol. **13**, 289–293 (2018).
[14]R. Mishra, W. Zhou, S. J. Pennycook, S. T. Pantelides, and J.-C. Idrobo, "Long-range ferromagnetic ordering in manganese-doped two-dimensional dichalcogenides," Phys. Rev. B **88**, 144409 (2013).
[15]A. Ramasubramaniam and D. Naveh, "Mn-doped monolayer MoS_2: An atomically thin dilute magnetic semiconductor," Phys. Rev. B Condens. Matter Mater. Phys. **87**, 195201 (2013).
[16]Y. C. Cheng, Z. Y. Zhu, W. B. Mi, Z. B. Guo, and U. Schwingenschlogl, "Prediction of two-dimensional diluted magnetic semiconductors: Doped monolayer MoS_2 systems," Phys. Rev. B **87**, 100401(R) (2013).
[17]Z. Zhang, X. Zou, V. H. Crespi, and B. I. Yakobson, "Intrinsic magnetism of grain boundaries in two-dimensional metal dichalcogenides," ACS Nano **7**, 10475 (2013).
[18]O. V. Yazyev and Y. P. Chen, "Polycrystalline graphene and other two-dimensional materials," Nat. Nanotechnol. **9**, 755 (2014).
[19]Y. Cai, H. Zhou, G. Zhang, and Y.-W. Zhang, "Modulating carrier density and transport properties of mos_2 by organic molecular doping and defect engineering," Chem. Mater. **28**, 8611 (2016).
[20]A. Vojvodic, B. Hinnemann, and J. K. Nørskov, "Magnetic edge states in MoS_2 characterized using density-functional theory," Phys. Rev. B **80**, 125416 (2009).
[21]A. N. Andriotis and M. Menon, "Tunable magnetic properties of transition metal doped MoS_2," Phys. Rev. B **90**, 125304 (2014).
[22]Q. Yue, Z. Shao, S. Chang, and J. Li, "Adsorption of gas molecules on monolayer MoS_2 and effect of applied electric field," Nanoscale Res. Lett. **8**, 425 (2013).
[23]Y. Li, Z. Zhou, S. Zhang, and Z. Chen, "MoS_2 nanoribbons: High stability and unusual electronic and magnetic properties," J. Am. Chem. Soc. **130**, 16739 (2008).
[24]M. P. K. Sahoo, J. Wang, Y. Zhang, T. Shimada, and T. Kitamura, "Modulation of gas adsorption and magnetic properties of monolayer-MoS_2 by antisite defect and strain," J. Phys. Chem. C **120**, 14113 (2016).
[25]J. He, K. Wu, R. Sa, Q. Li, and Y. Wei, "Magnetic properties of nonmetal atoms absorbed monolayers," Appl. Phys. Lett. **96**, 082504 (2010).
[26]M. Kan, S. Adhikari, and Q. Sun, "Ferromagnetism in MnX_2 (X=S, Se) monolayers," Phys. Chem. Chem. Phys. **16**, 4990 (2014).
[27]X. Lin and J. Ni, "Charge and magnetic states of Mn-, Fe-, and Co-doped monolayer MoS_2," J. Appl. Phys. **116**, 044311 (2014).

[28]S.-C. Lu and J.-P. Leburton, "Electronic structures of defects and magnetic impurities in MoS_2 monolayers," Nanoscale Res. Lett. **9**, 676 (2014).
[29]A. A. Tedstone, D. J. Lewis, and P. O'Brien, "Synthesis, Properties, and Applications of Transition Metal-Doped Layered Transition Metal Dichalcogenides," Chem. Mater. **28**, 1965 (2016).
[30]W.-F. Li, C. Fang, and M. A. van Huis, "Strong spin-orbit splitting and magnetism of point defect states in monolayer WS_2," Phys. Rev. B **94**, 195425 (2016).
[31]D. Gao, M. Si, J. Li, J. Zhang, Z. Zhang, Z. Yang, and D. Xue, "Ferromagnetism in freestanding MoS_2 nanosheets," Nanoscale Res. Lett. **8**, 129 (2013).
[32]S. Yan, W. Qiao, X. He, X. Guo, L. Xi, W. Zhong, and Y. Du, "Enhancement of magnetism by structural phase transition in MoS_2," Appl. Phys. Lett. **106**, 012408 (2015).
[33]L. Cai, J. He, Q. Liu, T. Yao, L. Chen, W. Yan, F. Hu, Y. Jiang, Y. Zhao, T. Hu, Z. Sun, and S. Wei, "Vacancy-induced ferromagnetism of MoS_2 nanosheets," J. Am. Chem. Soc. **137**, 2622 (2015).
[34]K. Zhang, S. Feng, J. Wang, A. Azcatl, N. Lu, R. Addou, N. Wang, C. Zhou, J. Lerach, V. Bojan, M. J. Kim, L.-Q. Chen, R. M. Wallace, M. Terrones, J. Zhu, and J. A. Robinson, "Manganese doping of monolayer MoS_2: the substrate is critical," Nano Lett. **15**, 6586 (2015).
[35]Z. C. Xiang, Z. Zhang, X. J. Xu, Q. Zhang, Q. B. Wang, and C. Yuan, "Room-temperature ferromagnetism in Co doped MoS_2 sheets," Phys. Chem. Chem. Phys. **17**, 15822 (2015).
[36]N. Huo, Y. Li, J. Kang, R. Li, Q. Xia, and J. Li, "Edge-states ferromagnetism of WS_2 nanosheets," Appl. Phys. Lett. **104**, 202406 (2014).
[37]J. Wang, F. Sun, S. Yang, Y. Li, C. Zhao, M. Xu, Y. Zhang, and H. Zeng, "Robust ferromagnetism in Mn-doped MoS_2 nanostructures," Appl. Phys. Lett. **109**, 092401 (2016).
[38]Y. Yu, S.-Y. Huang, Y. Li, S. N. Steinmann, W. Yang, and L. Cao, "Layer-dependent electrocatalysis of MoS_2 for hydrogen evolution," Nano Lett. **14**, 553 (2014).
[39]R. Peng, L. Liang, Z. D. Hood, A. Boulesbaa, A. Puretzky, A. V. Ievlev, J. Come, O. S. Ovchinnikova, H. Wang, C. Ma, M. Chi, B. G. Sumpter, and Z. Wu, "In-plane heterojunctions enable multiphasic two-dimensional (2D) MoS_2 nanosheets as efficient photocatalysts for hydrogen evolution from water reduction," ACS Catal. **6**, 6723 (2016).
[40]T. F. Jaramillo, K. P. Jørgensen, J. Bonde, J. H. Nielsen, S. Horch, and I. Chorkendorff, "Identification of active edge sites for electrochemical H_2 evolution from MoS_2 nanocatalysts," Science **317**, 100 (2007).
[41]Y. Xu, L. Wang, X. Liu, S. Zhang, C. Liu, D. Yan, Y. Zeng, Y. Pei, Y. Liuc, and S. Luo, "Monolayer MoS_2 with S vacancies from interlayer spacing expanded counterparts for highly efficient electrochemical hydrogen production," J. Mater. Chem. A **4**, 16524 (2016).
[42]Y. Yin, J. Han, Y. Zhang, X. Zhang, P. Xu, Q. Yuan, L. Samad, X. Wang, Y. Wang, Z. Zhang, P. Zhang, X. Cao, B. Song, S. Jin, Contributions of phase, and sulfur vacancies, and edges to the hydrogen evolution reaction catalytic activity of porous molybdenum disulfide nanosheets," J. Am. Chem. Soc. **138**, 7965 (2016).
[43]X. Dai, K. Du, Z. Li, M. Liu, Y. Ma, H. Sun, X. Zhang, and Y. Yang, "Co-Doped MoS_2 nanosheets with the dominant CoMoS phase coated on carbon as an excellent electrocatalyst for hydrogen evolution," ACS Appl. Mater. Interfaces **7**, 27242 (2015).
[44]G. Liu, A. W. Robertson, M. M.-J. Li, W. C. H. Kuo, M. T. Darby, M. H. Muhieddine, Y.-C. Lin, K. Suenaga, M. Stamatakis, J. H. Warner, and S. C. E. Tsang, "MoS_2 monolayer catalyst doped with isolated Co atoms for the hydrodeoxygenation reaction," Nat. Chem. **9**, 810–816 (2017).
[45]A. J. Appleby, "Electrocatalysis and fuel cells," Catal. Rev. **4**, 221–244 (1970).
[46]K. Kinoshita, *Electrochemical Oxygen Technology* (Wiley, New York, 1992).
[47]T. Toda, H. Igarashi, H. Uchida, and M. Watanabe, "Enhancement of the electroreduction of oxygen on Pt alloys with Fe, Ni and Co," J. Electrochem. Soc. **146**, 3750–3756 (1999).
[48]N. M. Markovic, V. Radmilovic, and P. N. Ross, in *Catalysis and Electrocatalysis at Nanoparticle Surfaces*, edited by A. Wieckowski, E. Savinova, and C. Vayenas (Marcel Dekker, New York, Basel, 2003), Chap. 9.
[49]S. Mukerjee and S. Srinivasan, "Enhanced electrocatalyssis of oxygen reduction reaction on platinum alloys in proton-exchange membrane fuel-cells," J. Electroanal. Chem. **357**, 201–224 (1993).
[50]R. R. Chianelli, G. Berhault, and B. Torres, "Unsupported transition metal sulfide catalysts: 100 years of science and application," Catalysis Today **147**, 275–286 (2009).
[51]J. G. Kushmerick, S. A. Kandel, P. Han, J. A. Johnson, and P. S. Weiss, "Atomic-scale insights into hydrodesulfurization," J. Phys. Chem. B **104**, 2980–2988 (2000).
[52]X. Wang, H. Fang, Z. Zhao, A. Duan, C. Xu, Z. Chen, M. Zhang, P. Du, S. Song, P. Zheng, and K. Chi, "Effect of promoters on the HDS activity of alumina supported Co–Mo sulfide catalysts," RSC Adv. **5**, 99706–99711 (2015).
[53]A. J. A. Konings, W. L. J. Brentjens, D. C. K. Koninhsberger, and V. H. J. De Beer, "ESR Studies on hydrodesulfurization catalysts: Nickel- or cobalt-promoted sulfided tungsten- or molybdenum-containing catalysts," J. Catalysis **67**, 145–158 (1981).
[54]B. Xia, Q. Guo, D. Gao, S. Shi, and K. Tao, "High temperature ferromagnetism in Cu-doped MoS_2 nanosheets," J. Phys. D Appl. Phys. **49**, 165003 (2016).
[55]S. Ahmed, X. Ding, N. Bao, P. Bian, R. Zheng, Y. Wang, P. P. Murmu, J. V. Kennedy, R. Liu, H. Fan, K. Suzuki, J. Ding, and J. Yi, "Inducing high coercivity in MoS2 nanosheets by transition element doping," Chem. Mater. **29**, 9066–9074 (2017).
[56]S. S. Rao, K. N. Anuradha, S. Sarangi, and S. V. Bhat, "Weakening of charge order and anti ferromagnetic to ferromagnetic switch over in $Pr_{0.5}Ca_{0.5}MnO_3$ nanowires," Appl. Phys. Lett **87**, 182503 (2005).
[57]K. N. Anuradha, S. S. Rao, and S. V. Bhat, "Complete melting of charge order in hydrothermally grown $Pr_{0.57}Ca_{0.41}$ $Ba_{0.02}MnO_3$ Nanowires," J. Nanosci. Nanotechnol. **7**, 1775 (2007).
[58]K. Gandha, K. Elkins, N. Poudyal, X. Liu, and J. Ping Liu, "High energy product developed from cobalt nanowires," Sci. Rep. **4**, 5345.
[59]L. M. Martinez, M. D. Teran, R. R. Chianelli, S. R. J. Hennadige, and S. R. Singamaneni, "Magnetic defects in transitional metal di-chalcogenide semiconducting layers," MRS Adv. **3**, 351–357 (2018).
[60]L. M. Martinez, C. Karthik, M. R. Kongara, and S. R. Singamaneni, "Paramagnetic defects in hydrothermally grown few-layered MoS_2 nanocrystals," J. Mater. Res. **33**, 1565 (2018).
[61]Y. Wu, M. Zarei-Chaleshtori, B. Torres, T. Akter, C. Diaz-Moreno, G. B. Saupe, J. A. Lopez, R. R. Chianelli, and D. Villagran, "Electrocatalytic hydrogen gas generation by cobalt molybdenum disulfide ($CoMoS_2$) synthesized using alkyl-containing thiomolybdate precursors," Int. J. Hydrogen Energy **42**, e20676 (2017).
[62]S. S. Rao, S. Narayana Jammalamadaka, A. Stesmans, V. V. Moshchalkov, J. van Tol, D. V. Kosynkin, A. Higginbotham, and J. M. Tour, "Ferromagnetism in graphene nanoribbons: Split versus oxidative unzipped ribbons," Nano Lett. **12**, 1210 (2012).
[63]J. Zhang, J. M. Soon, K. P. Loh, J. Yin, J. Ding, M. B. Sullivian, and P. Wu, "Magnetic molybdenum disulfide nanosheet films," Nano Lett. **7**, 2370 (2007).
[64]B. Xia, Y. Yang, J. Ma, K. Tao, and D. Gao, "Adjustable ferromagnetic behavior in iron-doped two-dimensional MoS_2 multilayer nanosheets," Appl. Phys. Express **10**, 093002 (2017).
[65]K. P. Bhatti, S. Chaudhary, D. K. Pandya, and S. C. Kashyap, "Intrinsic and extrinsic origin of room temperature ferromagnetism in ZnO:Co," J. Appl. Phys. **101**, 103919 (2007).
[66]D. Wang, X. Zhang, Y. Shen, and Z. Wu, "Ni-doped MoS_2 nanoparticles as highly active hydrogen evolution electrocatalysts," RSC Adv. **6**, 16656 (2016).
[67]S. Dong, X. Liu, X. Li, V. Kanzyuba, T. Yoo, S. Rouvimov, S. Vishwanath, H. G. Xing, D. Jena, M. Dobrowolska, and J. K. Furdyna, "Room temperature weak ferromagnetism in $Sn_{1-x}Mn_xSe_2$ 2D films grown by molecular beam epitaxy," APL Materials **4**, 032601 (2016).
[68]C.-S. Park, D. Chu, Y. Shon, J. Lee, and E. K. Kim, "Room temperature ferromagnetic and ambipolar behaviors of MoS_2 doped by manganese oxide using an electrochemical method," Appl. Phys. Lett. **110**, 222104 (2017).
[69]H. Wang, C. Tsai, D. Kong, K. Chan, F. Abid-Pederson, J. K. Nørskov, and Y. Cui, "Transition-metal doped edge sites in vertically aligned MoS_2 catalysts for enhanced hydrogen evolution," Nano Res. **8**, 566 (2015).
[70]J. Deng, H. Li, J. Xiao, Y. Tu, D. Deng, H. Yang, H. Tian, J. Li, P. Ren, and X. Bao, "Triggering the electrocatalytic hydrogen evolution activity of the inert two-dimensional MoS_2 surface via single-atom metal doping," Energy Environ. Sci. **8**, 1594–1601 (2015).
[71]X. Ren, L. Pang, Y. Zhang, X. Ren, and H. Fan, "One-step hydrothermal synthesis of monolayer MoS_2 quantum dots for highly efficient electrocatalytic hydrogen evolution," J. Mater. Chem. A **3**, 10693 (2015).
[72]K. Ojha, S. Saha, S. Banerjee, and A. K. Ganguli, "Efficient electrocatalytic hydrogen evolution from MoS_2-functionalized Mo_2N nanostructures," ACS Appl. Mater. Interfaces **9**, 19455–19461 (2017).
[73]R. Prins, V. H. J. De Beer, and G. A. Somorjai, "Structure and function of the catalyst and the promoter in Co – Mo hydrodesulfurization catalysts," Catal. Rev. **31**, 1–41 (1989).

[74]Z. W. Seh, J. Kibsgaard, C. F. Dickens, Ib Chorkendorff, J. K. Nørskov, and T. F. Jaramillo, "Combining theory and experiment in electrocatalysis: Insights into materials design," Science **355**, 146 (2017).
[75]D. Merki, H. Vrubel, L. Rovelli, S. Fierro, and X. H. Fe, "Co, and Ni ions promote the catalytic activity of amorphous molybdenum sulfide films for hydrogen evolution," Chem. Sci. **3**, 2515–2525 (2012).
[76]P. W. Selwood, "Magnetism and catalysis," Chem. Rev. **38**, 41–82 (1946).
[77]J. T. Richardson, "Magnetism and catalysis," J. Appl. Phys. **49**, 1781 (1978).
[78]R. J. H. Voorhoeve, "Experimental relationships between catalysis and magnetism," AIP Conf. Proc. **18**, 19 (2008).
[79]E. Torun, C. M. Fang, G. A. de Wijs, and R. A. de Groot, "Role of Magnetism in Catalysis: RuO_2 (110) Surface," J. Phys. Chem. C. **117**, 6353–6357 (2013).